The 9th European Congress on Computational Methods in Applied Sciences and Engineering
ECCOMAS Congress 2024
3 – 7 June 2024, Lisboa, Portugal

# STRAIN RATE SENSITIVE DELAMINATION MODELLING IN FIBRE REINFORCED POLYMER COMPOSITES

**JAKOV RATKOVIĆ[*] AND DARKO IVANČEVIĆ[†]**

[*] Department of Aeronautical Engineering
University of Zagreb Faculty of Mechanical Engineering and Naval Architecture
Ivana Lučića 5, 10000 Zagreb, Croatia
e-mail: jakov.ratkovic@fsb.unizg.hr, www.fsb.unizg.hr

[†] Department of Aeronautical Engineering
University of Zagreb Faculty of Mechanical Engineering and Naval Architecture
Ivana Lučića 5, 10000 Zagreb, Croatia
e-mail: darko.ivancevic@fsb.unizg.hr, www.fsb.unizg.hr

**Key words:** Composite, FRP, Interlaminar Damage, Delamination Modelling, Numerical Simulation, Strain Rate Effects

**Summary.** *The present work is focused on numerical modelling of the strain rate dependent interlaminar damage initiation and propagation in fibre reinforced polymer (FRP) composite materials. The numerical model is developed as a VUMAT user-defined material model subroutine implemented in the commercial finite element software Abaqus/Explicit. Results are validated against the Double Cantilever Beam (DCB) experiments performed in the available literature. The results obtained using the developed material model provide a satisfactory correlation compared to the experimental results.*

## 1 INTRODUCTION

In the out-of-plane impact events on the FRP plates, delamination, i.e., interlaminar damage is amongst the most significant failure modes that could lead to total failure of the composite structure [1-3]. Hence, in the everlasting motivation to reduce composite structures' development time and cost by performing high fidelity numerical simulations comprehensively describing the behaviour of FRP composite structures in all loading conditions and scenarios, it is necessary to accurately capture the delamination phenomena. Furthermore, such events frequently result in elevated strain rate conditions. As it has been shown in the literature, FRP composites, along with their interlaminar interfaces, exhibit strain rate dependence [4-6]. Thus, in this work, strain rate effects on interlaminar strength and fracture toughness are introduced, resulting in a strain rate dependent interlaminar damage initiation and propagation model.

In the thorough investigation of strain rate dependency of interlaminar composite properties, it was found that interlaminar strengths [2,4] fracture energies [3,4] and failure modes, i.e., mechanisms [7,8], are all rate dependent. Moreover, positive [9], negative [10], and indifferent [11] correlations of all of the mentioned properties were reported, which led to the conclusion

that at the present moment, no consensus on the topic has been reached yet [12]. Possible sources of the vast result discrepancies could be differences in material systems used, ranges of studied test rates, test configurations and data reduction methods, as well as in the possible errors in high rate load and displacement measurements [5,7].

Hence, in this initial study on the topic, an effort to improve the field of interlaminar rate dependency has been made. In this work, the opening displacement rate was taken as a referent rate dependency variable, i.e., the abscissa axis variable. The model presented in this study is currently under development. It is part of a wider research on carbon fibre epoxy material system strain rate dependent progressive damage modelling in high strain rate and impact loading regimes (e.g., previous study by the authors [13]). The numerical model is developed as a VUMAT user-defined material model subroutine implemented in commercial finite element software Abaqus/Explicit. It is utilized with the Abaqus built-in zero-thickness cohesive elements. Results are verified with the Abaqus built-in cohesive traction separation material model and are validated against the Double Cantilever Beam (DCB) experiments performed in the available literature. The results obtained using the developed material model show a satisfactory correlation when compared to the established Abaqus built-in model and experimental results.

## 2 METHODOLOGY

### 2.1. Material model development

Interface constitutive behaviour prior to damage initiation is defined as a standard decoupled traction-separation law:

$$\begin{Bmatrix} t_n \\ t_s \\ t_t \end{Bmatrix} = \begin{bmatrix} K_n & 0 & 0 \\ 0 & K_s & 0 \\ 0 & 0 & K_t \end{bmatrix} \cdot \begin{Bmatrix} \delta_n \\ \delta_s \\ \delta_t \end{Bmatrix}, \tag{1}$$

where the vector on the left side is a traction vector, while the matrix on the right side is a diagonal penalty stiffness matrix, which relates the displacement vector (on the right side of the equation) to the traction vector. In this formulation, strain components are related to element displacements with the following relations:

$$\varepsilon_n = \frac{\delta_n}{T_0}, \qquad \varepsilon_s = \frac{\delta_s}{T_0}, \qquad \varepsilon_t = \frac{\delta_t}{T_0}. \tag{2}$$

As the zero thickness cohesive finite elements were chosen to model interfacial behaviour, the assumption of unity of initial thickness $T_0$ is valid. Hence, Eq. (2) can be rewritten as follows:

$$\varepsilon_n = \delta_n, \qquad \varepsilon_s = \delta_s, \qquad \varepsilon_t = \delta_t. \tag{3}$$

Damage initiation is considered to be triggered once the interactive quadratic traction failure criterion has been met:

$$\left(\frac{\langle t_n \rangle}{N}\right)^2 + \left(\frac{t_s}{S}\right)^2 + \left(\frac{t_t}{T}\right)^2 \geq 1, \tag{4}$$

in which $N, S$ and $T$ are the normal and two shear interlaminar strengths, i.e., failure tractions, respectively. After damage initiation, the softening behaviour is modelled according to the linear degradation law as follows:

$$\begin{Bmatrix} t_n \\ t_s \\ t_t \end{Bmatrix} = \begin{bmatrix} \left(1 - D \cdot \frac{\langle \delta_n \rangle}{\delta_n}\right) K_n & 0 & 0 \\ 0 & (1-D)K_s & 0 \\ 0 & 0 & (1-D)K_t \end{bmatrix} \cdot \begin{Bmatrix} \delta_n \\ \delta_s \\ \delta_t \end{Bmatrix}. \quad (5)$$

From Eq. (4) and (5), it can be seen that compressive loading regime contributes neither to delamination initiation, nor its progressive evolution. The mixed-mode damage variable $D$ in Eq. (5) is determined from the total rupture equivalent displacement $\delta^f$, instantaneous equivalent displacement $\delta$ and failure initiation equivalent displacement $\delta^0$ by the following relation:

$$D = \frac{\delta^f}{\delta} \cdot \left(\frac{\delta - \delta^0}{\delta^f - \delta^0}\right). \quad (6)$$

Instantaneous and failure initiation equivalent displacements are calculated as vector sums of all displacement components, whereas the total rupture equivalent displacement is determined from the mixed-mode fracture energy $G^C$ and the mixed-mode traction $t^0$ at delamination initiation as follows:

$$\delta^f = \frac{2 \cdot G^C}{t^0}. \quad (7)$$

The mixed-mode traction at damage onset is determined as a vector sum of the traction components, where normal traction is considered only if it is positive. The mixed-mode fracture energy is determined by the Reeders law, as proposed by Heidari-Rarani and Sayedain in [14]:

$$\frac{G_T}{G_{Ic} + (G_{IIc} - G_{Ic})\left(\frac{G_{II}+G_{III}}{G_T}\right)^{\eta} + (G_{IIIc} - G_{IIc})\left(\frac{G_{III}}{G_{II}+G_{III}}\right)^{\eta}\left(\frac{G_{II}+G_{III}}{G_T}\right)^{\eta}} \geq 1, \quad (8)$$

where $G_{Ic}, G_{IIc}$ and $G_{IIIc}$ are the critical strain energy release rates, i.e., fracture energies, of Mode I, Mode II and Mode III, respectively. $G_{II}$ and $G_{III}$ are Mode II and Mode III works done by the crack shearing and tearing, whereas $G_T$ is the total work done by all three characteristic fracture modes. Element deletion is ordered when the damage variable reaches a value of 0.98.

### 2.2. Displacement rate dependency

In order to capture the strain rate effects accurately, the initial step is to remove any numerically obtained noise in the determination of current strain rate values, which are expected due to the nature of the explicit integration scheme [12]. In this study, a Low-pass filter-like algorithm is employed, similar to the one proposed by Hoffmann in [15]. It requires definition of two parameters, namely displacement rate threshold $\dot{\delta}_{\text{tsh}}$ and limit $\dot{\delta}_{\text{lim}}$ values.

The new current displacement rate component $i$ in time step $n$ is determined as a ratio of current displacement increment component $i$ and current time increment as follows:

$$\dot{\delta}_{i,n} = \frac{\Delta\delta_{i,n}}{\Delta t_n}, \qquad i = n, t, s. \quad (9)$$

If the increment of the displacement rate, i.e., absolute value of the difference of its value from previous and current time step is lower than the defined threshold value $\dot{\delta}_{\text{tsh}}$, no further

action is required. Otherwise, if it exceeds $\dot{\delta}_{\text{tsh}}$, it has to be processed according to the following law:

$$\Delta\dot{\delta}_{\text{proc}} = \begin{cases} \Delta\dot{\delta}_{\text{raw}}, & \Delta\dot{\delta}_{\text{raw}} \leq \dot{\delta}_{\text{tsh}}; \\ \dot{\delta}_{\text{tsh}} + \left(\dot{\delta}_{\text{lim}} - \dot{\delta}_{\text{tsh}}\right) \cdot \left(1 - e^{-\frac{\Delta\dot{\delta}_{\text{raw}} - \dot{\delta}_{\text{tsh}}}{\dot{\delta}_{\text{lim}} - \dot{\delta}_{\text{tsh}}}}\right), & \Delta\dot{\delta}_{\text{raw}} > \dot{\delta}_{\text{tsh}}. \end{cases} \tag{10}$$

Then, depending on the sign of the difference of the displacement rates from previous and current time steps, the processed value of the displacement rate increment is added to the displacement rate from the previous time step as follows:

$$\dot{\delta}_{\text{proc},n} = \begin{cases} \dot{\delta}_{\text{proc},n-1} - \Delta\dot{\delta}_{\text{proc}}, & \dot{\delta}_n - \dot{\delta}_{\text{proc},n-1} < 0; \\ \dot{\delta}_{\text{proc},n-1} + \Delta\dot{\delta}_{\text{proc}}, & \dot{\delta}_n - \dot{\delta}_{\text{proc},n-1} > 0. \end{cases} \tag{11}$$

Dynamic increase factors (DIFs) of interface strengths, i.e. failure tractions, and fracture energies are then determined according to the empirical logarithmic functions, as proposed by Liu et al. [2]:

$$\text{DIF}_{\text{prop}}\left(\dot{\delta}_i\right) = \begin{cases} 1, & \dot{\delta}_i \leq \dot{\delta}^{\text{ref}}; \\ 1 + c_{\text{prop}} \cdot \ln\left(\dfrac{\dot{\delta}_i}{\dot{\delta}^{\text{ref}}}\right), & \dot{\delta}^{\text{ref}} < \dot{\delta}_i < \dot{\delta}^{\text{lim}}; \quad i = n, t, s. \\ \text{DIF}_{\text{prop}}^{\text{max}}, & \dot{\delta}_i \geq \dot{\delta}^{\text{lim}}, \end{cases} \tag{12}$$

In the above equation, $c_{\text{prop}}$ is the strain rate parameter of the specific interface property, $\dot{\delta}^{\text{ref}}$ is the referent displacement rate value at which the quasi-static properties were obtained, whereas $\dot{\delta}^{\text{lim}}$ is the limit (highest) displacement rate value at which the dynamic properties were measured. A qualitative representation of the displacement rate dependent bilinear traction-separation law with both failure traction and fracture energy considered displacement rate sensitive is shown in Figure 1.

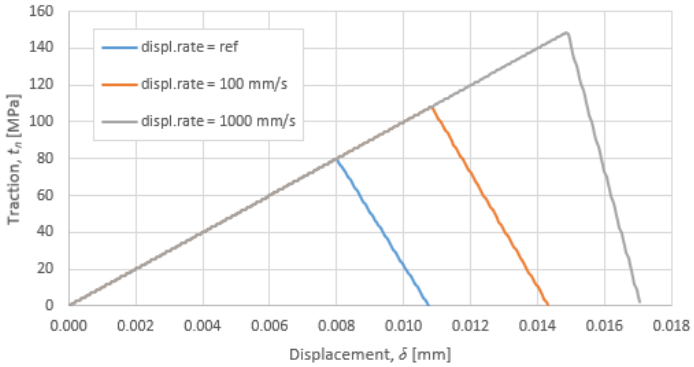


Figure 1. Displacement rate dependent bilinear traction separation law. Both interface strength (failure traction) and fracture energy are displacement rate sensitive

From Eq. (12), it can be seen that the DIFs, and thus the properties that they belong to, are capped below the referent and above the limit displacement rate values. This approach has been employed to reduce further uncertainties in the model, as also proposed by Hoffmann in [15].

## 2.3. Single cohesive element material model validation

Initial testing of the developed material model is performed on the simplest possible setup. A single zero thickness cohesive finite element (COH3D8) is embedded between two first order hexagonal finite elements with reduced integration (C3D8R). The model is tested in tensile and shear loading regimes. Sectioned simulation model is presented in Figure 2 a), while the same model with imposed loading and boundary conditions is depicted in Figure 2 b).

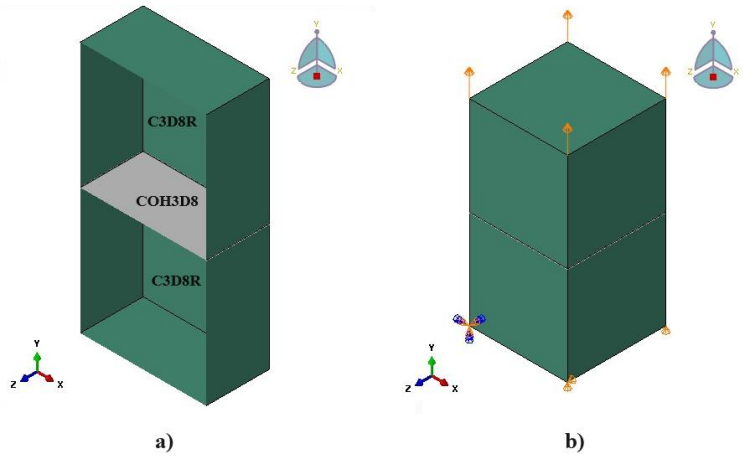


Figure 2. a) sectioned simulation model, b) imposed loading and boundary conditions

In this simplified numerical model that serves for verification purposes, linearly elastic isotropic material with properties $E$ =210 MPa, $\nu$ =0.3 and $\rho$ =7,800 kg/m$^3$ has been attributed to the C3D8R finite elements. The cohesive interface properties for these simple tests were chosen from a range of reported values for CFRP as $N = 80$ MPa, $S = T = 50$ MPa, $K_n = K_s = K_t = 5 \cdot 10^{14}$ N/m$^3$, $G_{Ic} = 430$ N/m, $G_{IIc} = G_{IIIc} = 1{,}250$ N/m, and $\rho = 1{,}200$ kg/m$^3$.

Results of the tensile single cohesive element test are provided in Figure 3 a), whereas the results of the shear test are shown in Figure 3 b).

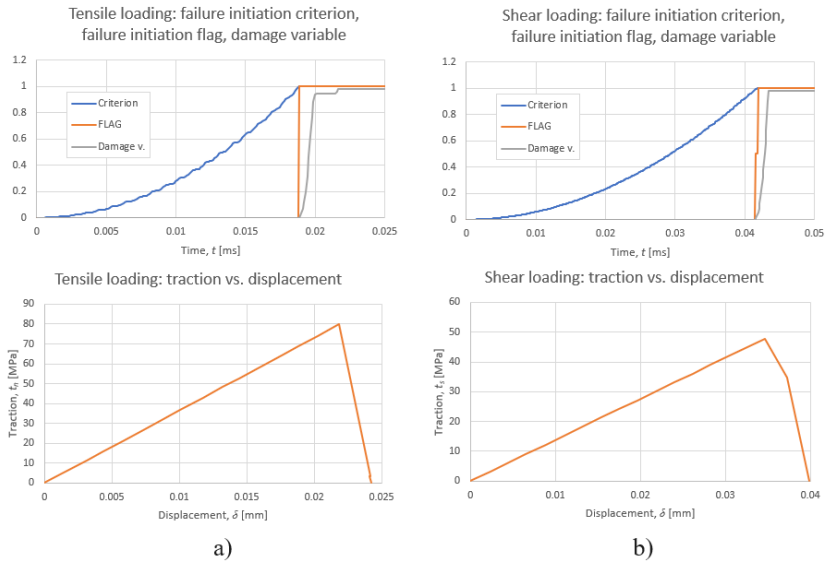


Figure 3. Model verification results using a single cohesive element: a) tensile loading, b) shear loading

In Figure 3 b), for the shear test, nonlinearity is visible in the post damage initiation part of the traction-separation envelope. This is simply the result of a loss of stability induced by the imposed boundary conditions in the shear test. The loss of stability results in tilting of the solid element, which further leads to modification of the equivalent displacement caused by an increase in tensile loading.

From the presented results, it can be concluded that the material model behaves as expected, which leads to further numerical investigation and testing of its validity in more complex problems.

## 3. NUMERICAL MODEL

Investigation of the Mode I behaviour was selected as the first step in the more complex evaluation of the developed model. Therefore, the Double Cantilever Beam (DCB) experiments performed by Zhang et al. in [1] were chosen to be replicated. In [1], double-beam specimens made of T700/MTM28-1 carbon epoxy unidirectional material system with a $[0_{24}/\text{PTFE}/0_{24}]$ layup were examined. The specimen dimensions were 80 x 15 x 6 mm, and a thin PTFE foil was inserted in the middle of the laminate over a length of 30 mm. In the reference, many different experiments were conducted corresponding to various crack propagation velocities. For simplicity reasons, in this study, only two different crack propagation velocities were considered, namely 108 m/s and 175 m/s.

The simulation model is shown in Figure 4 a), while the close-up view of the composite double-beam discretization is shown in Figure 4 b). Some elements were removed from the view in Figure 4 b) to better illustrate the modelling approach.

Composite beams were discretized as well by C3D8R finite elements with an approximate size of 0.2 x 0.5 x 0.75 mm. Along the solid finite elements representing the linearly elastic composite material, 7,500 zero thickness COH3D8 cohesive finite elements with average in-plane dimensions of 0.2 x 0.5 mm were used. This resulted in a total of 103,500 finite elements used to model the composite double beam. No Tie constraints were employed between composite solid and cohesive elements to improve computational efficiency. Instead, the separate meshes were connected by shared nodes.

The aluminum loading blocks were included in the model as well. They were connected to the composite beams by Tie constraints. Loading was defined as a displacement history taken from another work of the same research group [16]. Reference points were connected to the inner surfaces of the cylindrical holes in the aluminum adherends by the coupling constraints constraining every degree of freedom except for the rotation around the *y* axis. The blocks were discretized by first order hexagonal finite elements with reduced integration (C3D8R) with an average size of 0.5 mm, resulting in a total of 2,632 finite elements employed.

Simulations were performed using three different interface material models to gain insight into the validity of the developed material model, and to furthermore justify and test the necessity of the displacement rate effect modelling. Firstly, simulations were run using the developed material model. They are further denoted as “VUMAT with DIFs” simulations. Then, simulations were run using the developed model as well, but without dynamic effects, i.e., with all of the DIFs equal to one. These simulations are referred to as “VUMAT w/o DIFs”. Finally, simulations were run using the Abaqus in-built cohesive traction-separation law model, and these were denoted as “Abaqus model”.

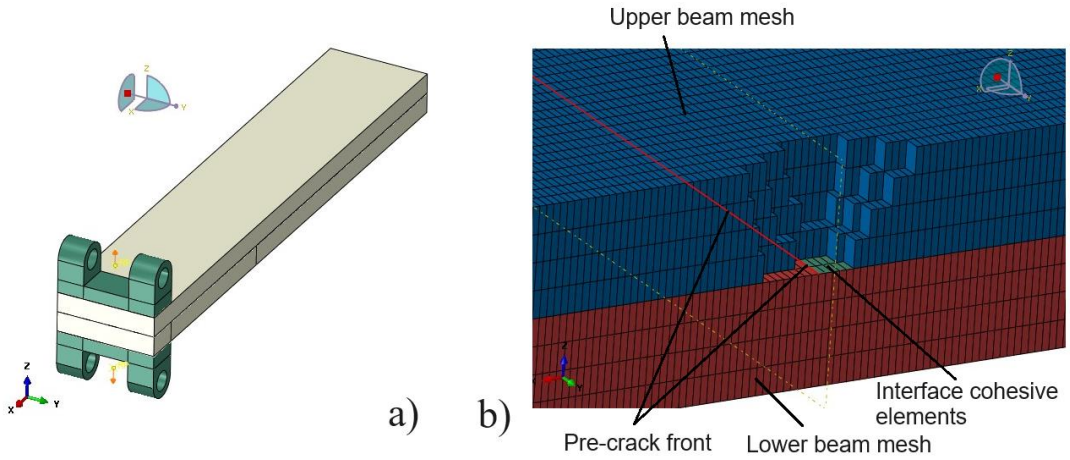


Figure 4. a) simulation model, b) close-up view of the composite double-beam discretization

Material properties for aluminum blocks are provided in Table 1, composite beam orthotropic linearly elastic material properties are given in Table 2, whereas the interface properties, along with the displacement rate parameters used in the "VUMAT with DIFs" simulations, are shown in Table 3.

Table 1. Aluminum block properties

| $E$ | $\nu$ | $\rho$ |
|---|---|---|
| [GPa] | [-] | [kg/m$^3$] |
| 70 | 0.32 | 2,700 |

Table 2. Composite beam material properties, [1]

| $E_1$ | $E_2 = E_3$ | $G_{12} = G_{13}$ | $G_{23}$ | $\nu_{12} = \nu_{13}$ | $\nu_{23}$ | $\rho$ |
|---|---|---|---|---|---|---|
| [GPa] | [GPa] | [GPa] | [GPa] | [-] | [-] | [kg/m$^3$] |
| 127 | 8.4 | 3.7 | 3 | 0.3 | 0.4 | 1,522 |

Table 3. Cohesive interface properties, [1,9]

| $K_n = K_s = K_t$ | $N_0 = S_0 = T_0$ | $\Gamma_{\mathrm{Ic}}^0$ | $\Gamma_{\mathrm{IIc}}^0 = \Gamma_{\mathrm{IIIc}}^0$ | $c_{N,S,T}$ | $m_{\Gamma\mathrm{Ic},\Gamma\mathrm{IIc},\Gamma\mathrm{IIIc}}$ | $\dot{\delta}_{\mathrm{ref}}$ | $\dot{\delta}_{\mathrm{lim}}$ |
|---|---|---|---|---|---|---|---|
| [N/m$^3$] | [MPa] | [N/m] | [N/m] | [-] | [-] | [mm/s] | [mm/s] |
| $5{\cdot}10^{14}$ | 80 | 430 | 1,250 | 0.22 | 0.5 | 20 | $10^5$ |

The resulting displacement rate dependencies of tensile strength (failure traction) and Mode I fracture energy are visually represented in Figure 5 a) and b), respectfully.

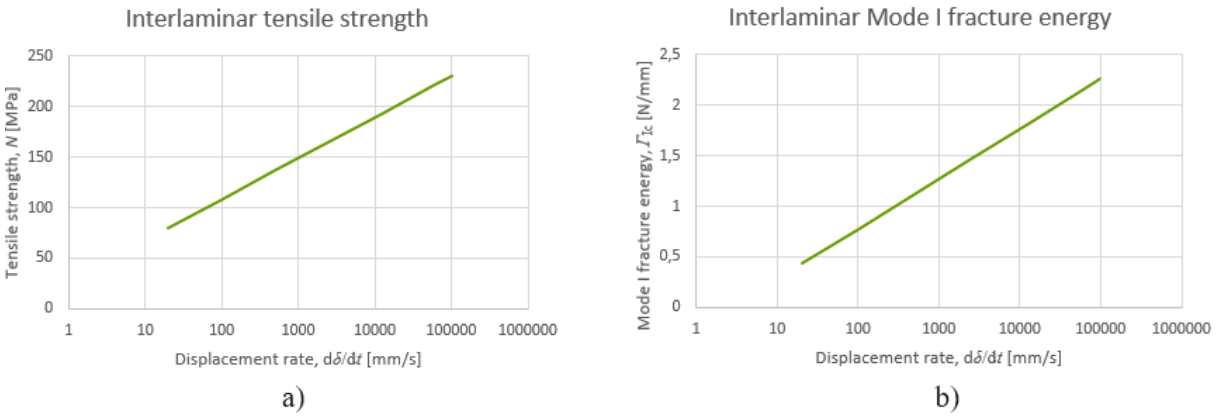


Figure 5. Displacement rate dependencies of: a) tensile failure traction, b) Mode I fracture energy

## 4. RESULTS

History plots of raw and processed displacement rate values for the 108 m/s and 175 m/s crack propagation velocities are given in the upper graphs in Figure 6. In the same figure, on the lower graphs, histories of corresponding dynamic values of failure traction and Mode I fracture energies are shown. From Figure 6 it can be concluded that the displacement rate processing algorithm is working properly and that the displacement rate sensitive interfacial properties are increased accordingly.

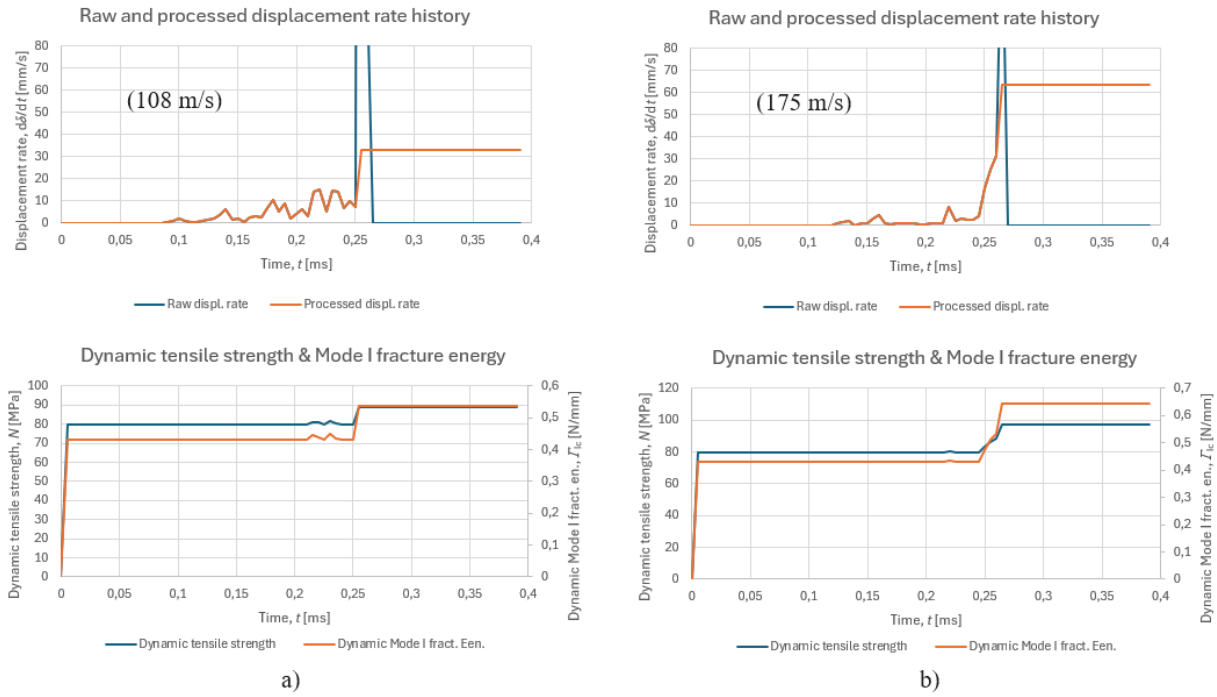


Figure 6. Time histories of raw and processed displacement rates (upper graphs) and dynamic failure tractions and Mode I fracture energies (lower graphs) for crack propagation velocities: a) 108 m/s and b) 175 m/s

Figure 7 presents a timelapse of failure initiation criteria distributions for the 108 m/s case,

for the defined three simulations using different interfacial material models. For the clarity of the results, Figure 7 shows only a close-up view of the interfaces instead of the full length of the model. The gray areas in these images represent initial interface geometry and therefore also mark the completely failed, i.e., deleted finite elements.

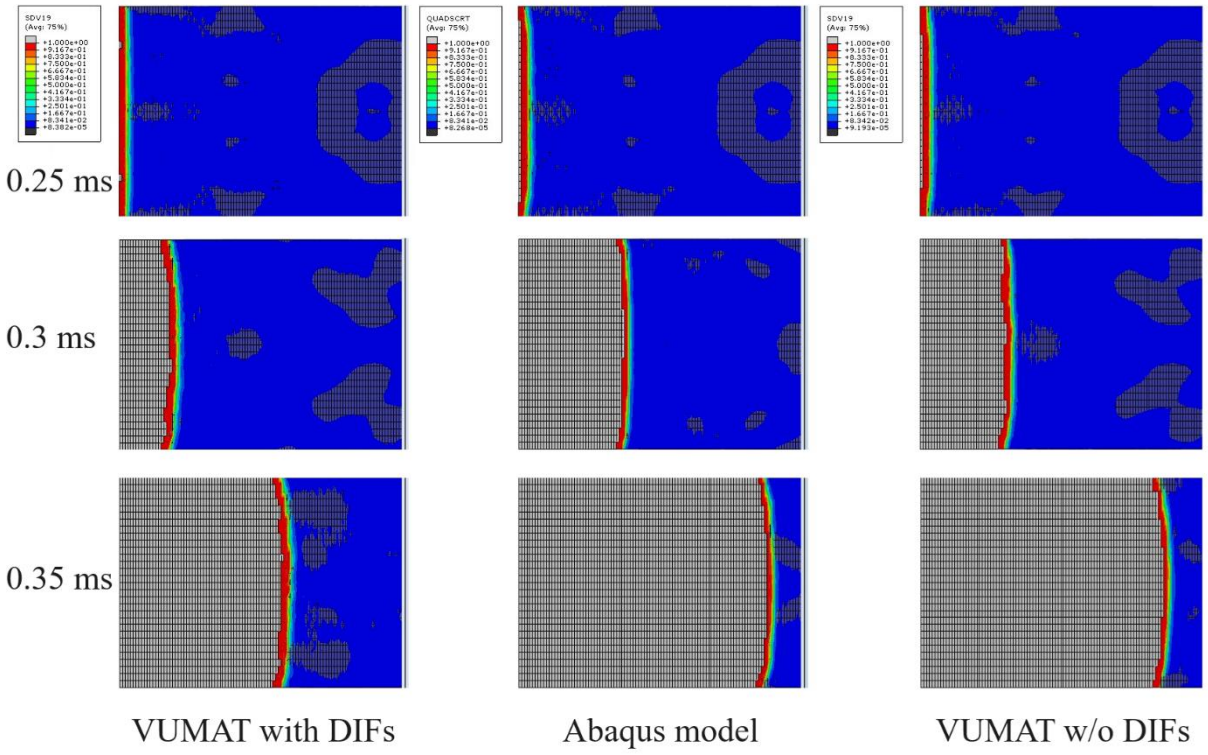


Figure 7. Timelapse of failure initiation criteria distributions for simulations using different interfacial material models

As shown in Figure 7, the differences between the results obtained by employing different material models are becoming more pronounced as the simulation time progresses. Comparison with the simulation results from the reference [1], it can be concluded that the model "VUMAT with DIFs" captures the delamination phenomena with closest resemblance to the referent results. However, in all of the simulations conducted in this study, the characteristic arc formation in the delamination front is present, which correlates well with numerical and experimental results from the literature.

Finally, comparison with experimentally obtained results is given by means of crack propagation velocities themselves. Figure 8 a) and b) provide comparisons of the crack propagation velocity histories for the 108 m/s and 175 m/s simulations, respectively.

As shown in Figure 8, in the case of the lower crack propagation velocity best correlation of results to the experimental ones is achieved by employing the here presented developed material model with inclusion of displacement rate effects. On the other hand, for the larger crack propagation velocity, better result correlation is achieved by utilization of Abaqus model and "VUMAT w/o DIFs", i.e., models with no displacement rate effects included. It is evident that all three models predicted delamination initiation with a delay. However, due to their too steep

crack propagation curve, models without displacement rate effects, which underestimate the dynamic Mode I fracture energy, show better general agreement with the experimental curve. Despite the larger overall discrepancy to the experimental results, the slope of the crack propagation envelope obtained using the "VUMAT with DIFs" material model is practically parallel to the experimentally obtained one. Possible explanation and more comments on these results are given in the following section.

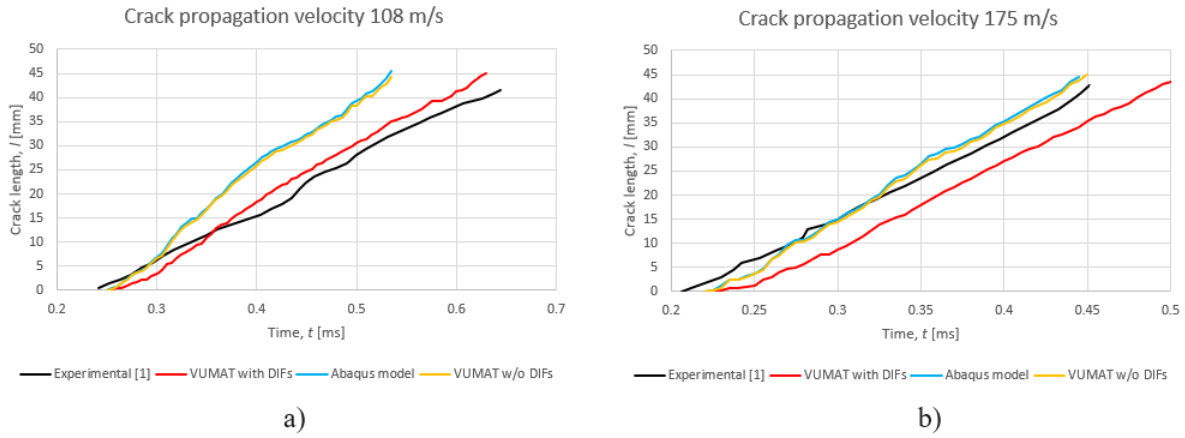


Figure 8. Crack propagation velocity histories: a) 108 m/s, b) 175 m/s

## 5. DISCUSSION

From Figure 6, it is clearly visible that the opening displacement rate at which the failure is initiated for the examined element is higher in the case of crack propagation velocity of 175 m/s than for the 108 m/s case. On the other hand, even for the 108 m/s, the displacement rates are elevated, and interface properties are increased accordingly. Hence, assuming that the experiment conducted is representative and that no numerical flaws are encountered in the simulations, it can only be concluded that the assumption of a consistent increase of both opening failure traction and Mode I fracture energy is incorrect.

Thus, it is necessary to obtain a more comprehensive compilation of experimental data for the interlaminar properties. It is crucial to generate reliable, strain rate sensitive data on a wider range of examined rates for a consistent material system. This experimental campaign needs to be performed for both relevant fracture modes - Mode I and Mode II, and even for Mixed mode at various mode mixity ratios.

Next, given that the reported trends in the literature, e.g. [3,6,9,10], are clearly non monotonic, implementation of more complex empirical functions should be considered to capture the strain/displacement rate effects.

Furthermore, sensitivity of the solution to the length of finite elements should be considered. It is well known that the process zone in the carbon fibre epoxy resin material systems is in the range of 1 - 4 mm and the numerical process zone should thus include at least 3 - 5 finite elements, as reported in e.g. [12]. The current model includes approximately 5 finite elements for a 1 mm process zone, however, sensitivity to element size and its correlation to strain rate dependent interlaminar strength, i.e., failure initiation tractions, will be evaluated in the continuation of this research.

Finally, in this study, all the material properties were considered to be dependent only on the opening displacement rate. Therefore, investigation of the possibility, i.e., the necessity, of correlating Mode II properties with the shearing displacement rate needs to be performed as well.

## 6. CONCLUSION

In this study, following a brief introduction to the topic, the developed displacement rate sensitive interfacial material model has been presented. It was created according to recent findings in the published literature and was developed based on the conventional bilinear traction separation law. After testing it in the most fundamental numerical problems, i.e., single cohesive element tests, the developed model has been examined in the fracture Mode I by simulating the DCB test. The obtained results were compared to those numerically and experimentally obtained in the literature. The results comparison has proven its physical validity when tested against the Abaqus in-built model and has pointed out to certain agreements with dynamic experimental results. Furthermore, the comparison has shown that the results obtained with the here presented developed model are superior to the Abaqus quasi-static model in certain conditions, as well as it has revealed some potential issues to be dealt with in the upcoming phases of model development.

The key issues that are considered as possible sources of result discrepancies have been identified in the Discussion section. Future research therefore consists primarily of obtaining a more detailed and comprehensive experimental dataset. Along this, examination of influences of various model parameters, such as cohesive process zone length, displacement rate function shape and relevance of other displacement components for the rate effects will be carried out. Implementation of all of the mentioned improvements and considerations will, from authors' opinion, lead to substantially more high-fidelity model and thus more accurate results.

## ACKNOWLEDGEMENTS

The research is fully funded by the Croatian Science Foundation (HRZZ) within the project "Computational Modelling of Composite Structures Impact Damage" (CONCORDE), grant number UIP-HRZZ-2020-02-9317.

## REFERENCES

[1] Zhang, C., Liu, H., Cao, J. et al. 2021. Rate-Dependent Cohesive Models for Dynamic Mode I Interfacial Propagation and Failure of Unidirectional Composite Laminates. Coatings 11, no. 2 (January/February): 191. https://doi.org/10.3390/coatings11020191

[2] Liu, Y., van der Meer, F.P., Sluys, L.J. 2018. Cohesive zone and interfacial thick level set modeling of the dynamic double cantilever beam test of composite laminate, Theor Appl Fract Mec 96, (August): pp. 617-630. https://doi.org/10.1016/j.tafmec.2018.07.004

[3] Riezzo, M.A., Simmons, M., Russell, B. et al. 2019. Dynamic characterisation of interlaminar fracture toughness in carbon fibre epoxy composite laminates. Compos Part A 126, (November): 105597. https://doi.org/10.1016/j.compositesa.2019.105597

[4] Ma, L., Liu, F., Liu, D. et al. 2021. Review of Strain Rate Effects of Fiber-Reinforced Polymer Composites, Polymers 13, no. 17 (August): 2839. https://doi.org/10.3390/polym13172839
[5] Ekhtiyari, A., Alderliesten, R. Shokrieh, M.M. 2021. Loading rate dependency of strain energy release rate in mode I delamination of composite laminates, Theor Appl Fract Mec 112, (April): 102894. https://doi.org/10.1016/j.tafmec.2021.102894
[6] Zabala, H., Aretxabaleta, L., Castillo, G. et al. 2015. Loading rate dependency on mode I interlaminar fracture toughness of unidirectional and woven carbon fibre epoxy composites. Compos Struct 121, (March): pp. 75-82. https://doi.org/10.1016/j.compstruct.2014.11.001
[7] Chen, Y., Liu, K., Xu, Z. et al. 2023. A comprehensive experimental investigation of the rate-dependent interlaminar delamination behaviour of CFRP composites, Compos Part B 261, (July): 110788. https://doi.org/10.1016/j.compositesb.2023.110788
[8] Low, K.O., Johar, M., Israr, H.A. et al. 2021. Displacement Rate Effects on the Mode II Shear Delamination Behavior of Carbon Fiber/Epoxy Composites. Polymers 13, no. 11 (May/June): 1881. https://doi.org/10.3390/polym13111881
[9] Liu, H., Nie, H., Zhang, C. et al. 2018. Loading rate dependency of Mode I interlaminar fracture toughness for unidirectional composite laminates. Compos Sci Technol 167, (October): pp. 215-223. https://doi.org/10.1016/j.compscitech.2018.07.040
[10] Perry, J., Walley, S.M. 2022. Measuring the Effect of Strain Rate on Deformation and Damage in Fibre-Reinforced Composites: A Review. JDBM 8, (February): pp. 178-213. https://doi.org/10.1007/s40870-022-00331-0
[11] Weng, F., Fang, Y., Ren, M. et al. 2021. Effect of High Strain Rate on Shear Properties of Carbon Fiber Reinforced Composites. Compos Sci Technol 203, (February): 108599. https://doi.org/10.1016/j.compscitech.2020.108599
[12] B. G. Falzon. 2022. Computational modelling of the crushing of carbon fibre-reinforced polymer composites. Philos Trans A Math Phys Eng Sci 380, no. 2232 (August): 20210336. https://doi.org/10.1098/rsta.2021.0336
[13] Ivančević, D., Ratković, J., Giannaros, E. 2024. Strain rate-dependent failure modelling of impact damage in laminated CFRP structures. Compos Struct 330, (February): 117817. https://doi.org/10.1016/j.compstruct.2023.117817
[14] Heidari-Rarani, M., Sayedain, M. 2019. Finite element modeling strategies for 2D and 3D delamination propagation in composite DCB specimens using VCCT, CZM and XFEM Approaches. Theor Appl Fract Mec 103, (October): 102246. https://doi.org/10.1016/j.tafmec.2019.102246
[15] Hoffmann, J. *An investigation into the characterisation and modelling of the impact response of CFRP*. Exeter College, University of Oxford, Oxford, 2018.
[16] Liu, H., Meng, X., Zhang, H. et al. 2019. The dynamic crack propagation behavior of mode I interlaminar crack in unidirectional carbon/epoxy composites. Eng Fract Mech 215, (June): pp. 65-82. https://doi.org/10.1016/j.engfracmech.2019.05.004